Path Planning of Robot Fleet in Upside-Down Configuration

Matteo Formigli, Lorenzo Bonin, Paolo Gallina, and Stefano Seriani(✉)

Department of Engineering and Architecture, University of Trieste, Trieste, Italy
sseriani@units.it

Abstract. This article describes a new pick-and-place robotic system based on the use of upside-down robots: robots capable of climbing up walls or moving on ceilings in upside down. This configuration could offer an alternative to the use of delta robots. The fleet of robots is capable to pick some objects transported by a conveyor belt and download them in an unload area. Compared to delta robots, upside-down robots can move on a wider workspace and the configuration is scalable. A planning strategy for the upside-down robot fleet is presented. The identified algorithm has been simulated and its potential has been highlighted.

Keywords: Mobile robots · Climbing robots · Path planning · Pick and place

1 Introduction

In this paper we propose a new robotic paradigm for the pick and place of small and light objects from a conveyor belt [1]. Even if delta robots are particularly suited for pick and place applications [2–4], they need additional space over the workspace, which can be critical. Moreover, due to the fact that delta robots are stationary, the workspace where they can operate is limited. Additionally, in multi-layer conveyor systems, the passage between layers has to be produced with dedicated equipment, e.g. elevators.

The solution proposed in this paper is an alternative to delta robots to overcome the situations described before. It is based on multiple mobile platforms capable of climbing on walls and other tilted surfaces. Climbing robots can be employed for maintenance, inspection and diagnosis [5]. In this regard, several different adhesion methods are possible: grasping, vacuum or suction cups, bio-inspired methods [6,7], compliant mechanisms [8], and magnetic adherence [9].

Wall climbing robots based on magnetic force are the best candidates for widespread industrial applications. Indeed, permanent magnets have several advantages: passive reliability, low cost and the fact of being not powered [10,11]. These systems work very well when the surfaces to climb are made up out of ferromagnetic materials [12,13], as shown in Fig. 1a. As an alternative, robots can adopt magnetic wheels that combine locomotion and adhesion [14,15] (Fig. 1b).

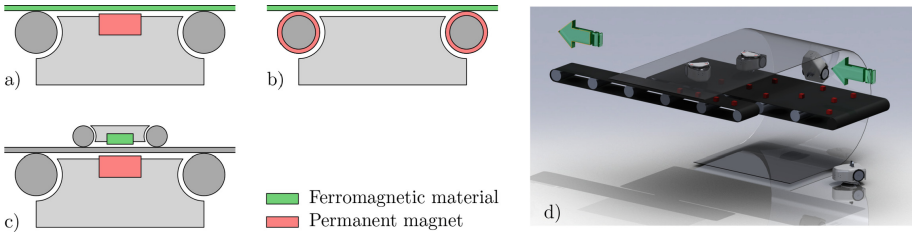

Fig. 1. Magnetic adhesion methods for mobile robots: a) a magnet is used to create adhesion between the robot and a ferromagnetic surface; b) magnetic wheels; c) sandwich configuration. In d) a rendering of the robotic scenario depicted in c) is shown.

When there is a non-ferromagnetic surface, a robot composed of two modules can be used: a *master* and a *follower* cart (Fig. 1c) arranged in a sandwich configuration. The stack is made up of the follower cart, the surface to climb and the master cart, which allows the robot to climb on non-ferromagnetic and curved surfaces; moreover, the master cart is capable of freely moving on the floor by detaching from the follower [16]. In the following we will refer to these robots as *upside-down robots*.

The proposed solution involves using a fleet of slow, small and simple mobile robots that, trough collaboration, can carry out the same task. A possible scenario is shown in Fig. 1d. Several upside-down robots have to pick some defected workpieces and place them on an unload conveyor belt. From time to time, some robots can change level floor by moving along the curved lateral surface.

With respect to delta robots, such a robotics paradigm offer several advantages:

- Thanks to the planar mobility of each upside-down robot, its workspace is theoretically unlimited.
- The robots can move from one layer to another by climbing curved connecting surfaces.
- Thanks to robot redundancy, the pick-and-place task is robust. If one robot has a failure, it can be replaced by the others.
- The system is scalable. If the conveyor throughput increases, new robots can be added.

Additionally, in a scenario where a network of delta robots is used, the problem of passing the objects from one robot to the other becomes critical. Conversely, this problem is not relevant in the case we propose, since the robots of the fleet are able to transport the objects from grasping to release, without interruption.

The paper is organized as follows. In Sect. 2 the algorithm that defines the robot movement strategy is defined. In Sect. 3 simulations are implemented and results are provided in Sect. 4. Thanks to the analysis of preliminary results it was possible to improve the algorithm and define the main features of the adopted approach. Finally, conclusions are presented and discussed.

2 Theoretical Model

The simulated world was constructed as a two dimensional kinematics representation of the environment in which the robots operate. Dynamics was omitted in order to keep computing time under control.

The simulated world is composed by two main elements: the *conveyor belt* and the *navigation surface*. The former transports the *items*. The robots are attached to the latter in an upside-down configuration. The *navigation area* is the projection of the navigation surface on reference plane.

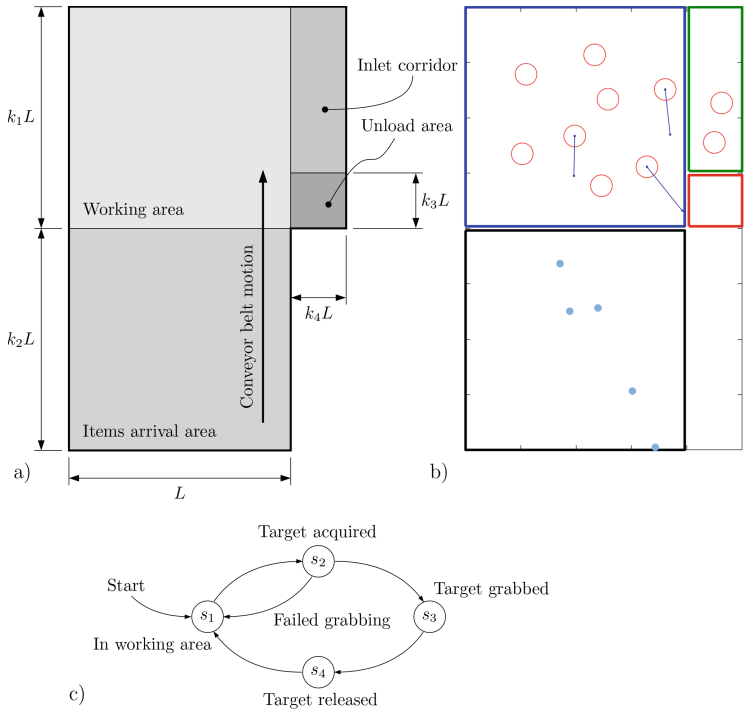

Fig. 2. Simulated environment and agent logic. a) Schematic representation. b) Graphical representation of robot footprints and items. c) State machine diagram.

The conveyor belt covers the areas named *working area* and *items arrival area*. The former represents the area in which the robots can pick the items transported by the conveyor belt. The latter is the section of the conveyor belt which is not covered by the navigation area.

The navigation area is composed of the working area, the *inlet corridor* and the *unload area*. After a robot picks an item, its new target position will become the unload area, where the item will be dropped. After the dropping, the robot reaches the working area moving through the inlet corridor. All the dimensions

of the simulated world are expressed in relation to the width of the conveyor belt L by means of the constants k_1, k_2, k_3 and k_4 and are visible in Fig. 2a. The view of the observer is visible in Fig. 2b.

Each agent is a differential drive robot and is assumed capable of motion in any direction. We consider a simplified kinematic model that doesn't consider proper non-holonomic constraints. Each agent is indicated as a red circle, as visible in Fig. 2b, with a footprint diameter of $0.1 \times L$.

Items are indicated as light-blue dots moving upwards, starting from the bottom of the items arrival area towards the top edge of the working area (see Fig. 2b).

The control system of the fleet is based around a computer vision system that tracks the position of each agent and item.

The implementation of the robot behaviour was made using a four-states *Finite-State Machine* (FSM), shown in Fig. 2c and described in the following sections.

2.1 State s_1: The Robots Uniformly Cover the Working Area

When in state s_1, the robot moves towards area free of robots, thus distributing uniformly on the working area. This strategy aims to avoid such situations where all the robots are far away from an item to pick. A local policy is implemented for each robot, which leads to the emerging of the wanted global behaviour.

An *area of obstacles perception* is defined around each $i-th$ robot (see Fig. 3a). It is delimited by a circle of radius r_{perc} and is centered on the robot center $\mathbf{P}_i = (x_i, y_i)$. During the state s_1, the robot moves considering only the n_p robots inside this area positioned at $\mathbf{P}_{p,l}$, for $l = \{1, ..., n_p\}$. For each, the distance $d_{il} = \|\mathbf{P}_i - \mathbf{P}_{p,l}\|$ allows to calculate a virtual force acting on the robot, as follows,

$$\mathbf{F}_{il} = \frac{\mathbf{P}_i - \mathbf{P}_{p,l}}{\|\mathbf{P}_i - \mathbf{P}_{p,l}\|} f(d_{il}, r_{perc}) \tag{1}$$

where $f(d, r)$ is zero if $d > r$ and $1/d$ otherwise.

For the $i-th$ robot to stand clear of the $s-th$ edge, the virtual forces $\mathbf{F}_{e,is}$ are introduced (see Fig. 3b). In case of the 1st wall, for example:

$$\mathbf{F}_{e,i1} = \Phi_s(WA, \mathbf{P}_i, r_{perc}) = \begin{cases} [0, f(y_i, r_{perc})] & if\ y_i < r_{perc} \\ [0, 0] & if\ y_i \geqslant r_{perc} \end{cases} \tag{2}$$

where WA refers to the working area.

By adding up all the contributions, the total force acting on the robot is given by:

$$\mathbf{R}_i = \sum_{l=1}^{n_p} \mathbf{F}_{il} + \sum_{s=1}^{4} \mathbf{F}_{e,is} \tag{3}$$

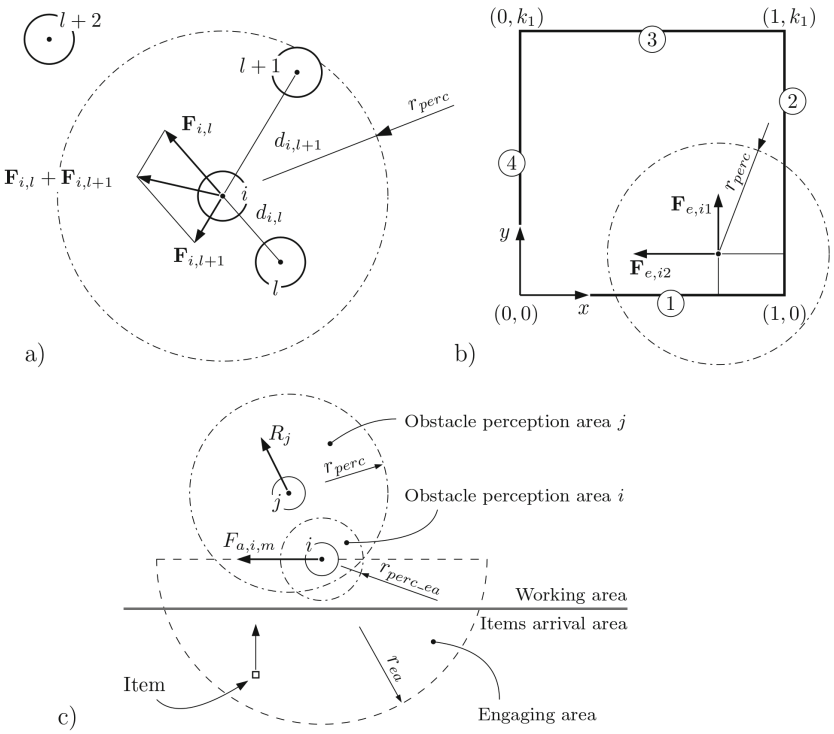

Fig. 3. Forces produced on the robots and interactions. a) Calculated forces in state s_1. b) Forces produced when the robot approaches the edges. c) Interaction between a robot in state s_2 and a robot in state s_1.

Since the movements of the robots are also simplified imposing a constant velocity v_c and instantaneous acceleration, the resulting force $\mathbf{R}_i$ affects only the direction of motion. Therefore, the velocity of the robot is given by:

$$\mathbf{v}_i = \begin{cases} (\mathbf{R}_i \;/\; \|\mathbf{R}_i\|)v_c \; if \; \mathbf{R}_i \neq [0,0] \\ 0 \; if \; \mathbf{R}_i = [0,0] \end{cases} \tag{4}$$

2.2 State s_2: The Robot Engages the Item

When the robot is on state s_2, it is engaging a specific item. Graphically, the engagement is represented by the blue solid line segment that connects the robot center to the engaged item (see Fig. 2b). Two conditions must be concurrently met for the robot to switch from state s_1 to s_2.

Condition 1. The item to pick enters the radius r_{ea} engaging area (see Fig. 3c).

Condition 2. The number of robots concurrently engaging the same item is lower than the specified maximum n_{eng_max}.

When the robot switches to state s_2, it moves in order to catch the item with the following force,

$$\mathbf{F}_{a,im} = [k_a(x_m - x_i), 0] \tag{5}$$

where i refers to the i-*th* robot and m to the m-*th* item that has been engaged. x_m and x_i are respectively the horizontal coordinates of the engaged item and of the robot center. k_a is a constant. This way the driving force is equivalent to the one produced by a spring of stiffness k_a.

Also during the state s_2, the motion of the robot is ruled by virtual forces similar to those provided by Eq. 1, but the area of obstacle perception is reduced. Its radius is r_{perc_ea}, where $r_{perc\_ea} < r_{perc}$, and the repulsive force is similarly defined.

The size difference of the obstacle perception area in the two states produce a positive global effect: robots in state s_1 move away from robots in state s_2, giving a higher priority to the task s_2. The full resultant force is given by:

$$\mathbf{R}_i = \sum_{l=1}^{n_p} \mathbf{F}_{il} + \sum_{s=1}^{4} \Phi_s(WA, \mathbf{P}_i, r_{perc\_ae}) + \mathbf{F}_{a,im} \tag{6}$$

As for state s_1, the resulting force $\mathbf{R}_i$ is used to calculate the instant speed of the robot according to Eq. 4.

A robot in state s_2 can return to state s_1 in two cases: if another robot picks the item; or if the item reaches a vertical position higher than the robot vertical position y_i before the robot manages to intercept its trajectory. In this last case, the robot loses the item, but the same item could be picked by an other robot later on.

The robot picks the item when it enters a small circular area centered on the robot's center, called *grasping area*. When this occurs, the robot switches to the state s_3.

2.3 State s_3: The Robot Moves to the *Unload Area*

In this state, the goal of the robot is to reach the *unload area*. This is implemented via an attractive force towards the goal,

$$\mathbf{F}_{u,i} = c_{ua} \frac{\mathbf{U} - \mathbf{P}_i}{\|\mathbf{U} - \mathbf{P}_i\|} \tag{7}$$

where c_{ua} is a constant and $\mathbf{U}$ is the barycenter of the unload area.

The obstacle perception area has the same size as in state s_2. This allows the robot to reach the unload area passing trough a crowd of s_1 state robots. These robots tend to move away from the robots in state s_3.

The repulsive forces produced by the edges of the navigation area are defined similarly to those as of Eq. 2, by considering the navigation area NA. Similarly to the other states, the resulting force $\mathbf{R}_i$ is used to calculate the actual speed of the robot according to Eq. 4. Once the robot reaches the unload area, it automatically unloads the item and increases the counter of collected items. After that, its state switches to s_4.

2.4 State s_4: The Robot Enters the Working Area Moving Along the Inlet Corridor

The state s_4 is the only one that allows a robot to use the *inlet corridor*. This was obtained by the attractive force

$$\mathbf{F}_{ic,i} = c_{ic} \frac{\mathbf{I} - \mathbf{P}_i}{\|\mathbf{I} - \mathbf{P}_i\|} \tag{8}$$

where c_{ic} is a constant and I is a waypoint located to the top of the inlet corridor. The resulting force $\mathbf{R}_i$ is used to calculate the actual speed of the robot according to Eq. 4.

3 Simulation

A large number of parameters influences the behaviour of the robotic fleet. To study their impact, multiple simulations were run with different parameter settings. For each combination of parameters, 7 different simulations were run in order to improve statistical significance. The *global evaluation value* g_e is given by the mean ratio between the n_lost_f lost items to the n_tot_f total number of items across the 7 simulations as follows:

$$g_e = \frac{1}{7} \sum_{i=1}^{7} \frac{n\_lost_f}{n\_tot_f} \tag{9}$$

The g_e value must be as low as possible.

At the beginning of each simulation, each agent in the fleet is positioned randomly in the working area by avoiding overlapping, following an uniform distribution. Items spawn at the bottom of the environment with random spatial and temporal distributions. More specifically, items spawn following a uniform distribution, while a normal distribution was used for timing the spawning.

In order to allow to compare configurations where different numbers of robots are generated in the working area WA, we linked the perception radius r_{perc} of the robots to the number of robots n_{robots} in the fleet. If OPA is the obstacle perception area, then,

$$OPA = \frac{WA}{n_{robots}}, \quad \text{and} \quad r_{perc} = \sqrt{\frac{OPA}{\pi}}. \tag{10}$$

4 Simulated Results

In this section we study the influence of the parameter n_{robots}, i.e. the number of robots in the fleet, on the performance of the system in terms of lost items. The main parameter values are shown in Table 1.

Table 1. Simulated world parameters.

	Parameter	Default value
Simulated world	n_{robots}	16
	μ	4 s
	σ	2 s
	sps	20
Robot	r_{ea}	$0.3 \times L$
	v_{max}	$0.1 \frac{L}{s}$
	$n_{targeting\_robots}$	1

The number of robot operating on the working area is progressively increased from 4 to 34. The aggregated results of the 7 simulations are presented in Fig. 4a.

As expected, the number of lost items decreases with increasing number of robots. A fleet of 16 robots is capable to intercept all the items transported by the conveyor belt.

At the same time it is reasonable to expect the number of lost items to increase dramatically when the number of robots is too high. This is because robots no longer have available space to move properly, getting in each other's way.

What is less evident is the high variability of the results when the number of robots is 32. This situation is well represented in Fig. 4b which usually happens when a robot captures an object in the upper part of the working area. On its way to the unload area it is pushed into the inlet corridor, moving against the normal flow, which leads to congestion; in fact, this effect can spiral out of control.

The high variability is due to the unpredictability of this effect, which may happen or not during any one simulation. In *simulation 7*, with a fleet of 30 robots, due to this behavior, the percentage of lost objects was 41.8%.

To solve this problem, a rule has been introduced which prevents robots in state s_3, i.e. which have just discarded an item, from entering the inlet corridor. Results of this new strategy are presented in Fig. 4a.

The system is reliable from fleets of 14 robots up to a fleet of 30 robots. With larger fleets the system performances decreases due to overcrowding of the working area: robots are unable to move fast enough to intercept in time the trajectory of their engaged items.

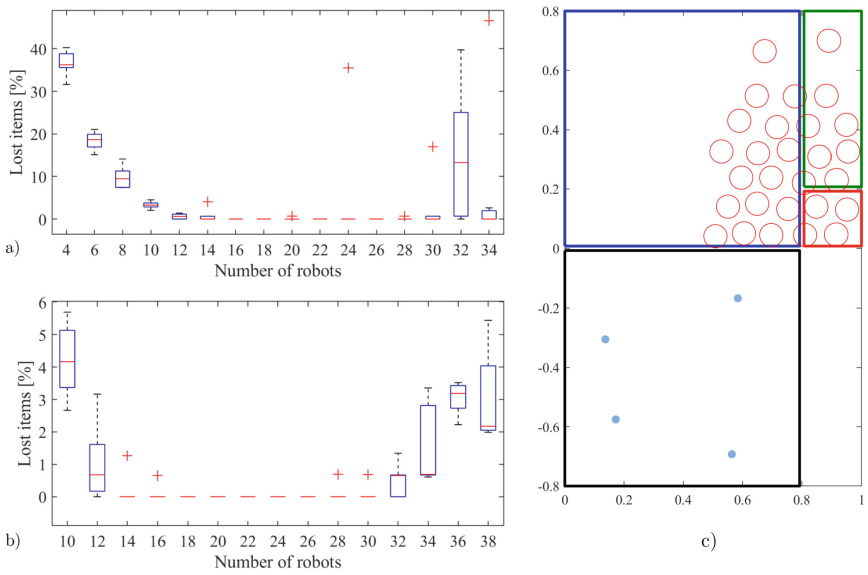

Fig. 4. Results of the simulations: a) Boxplot of the lost items vs the number of robot employed in the simulation. b) The lost items ratio when s_3 state robots are prevented from entering the inlet corridor. c) Simulated environment at the instant when the flow of robots is congested around the unload area.

5 Conclusions

This article described a new pick-and-place robotic configuration based on the use of upside-down robots: robots capable of climbing up walls or moving on ceilings in upside down. The fleet of robots is capable to pick some objects transported by a conveyor belt and download them in an unload area.

A control strategy for the upside-down robot fleet has been presented. The identified algorithm has been simulated and its potential has been highlighted.

The simulation has demonstrated the effectiveness of the strategy. Moreover, it has allowed to understand the influence of the various parameters involved in the overall robot fleet behaviour.

Acknowledgements. This research was supported by the University of Trieste - University funding for scientific Research projects - FRA 2018, the LAMA FVG project and the PRIN 2017 project "SEDUCE" n. 2017TWRCNB from the Italian Ministry of University and Research.

References

1. Karimi Eskandary, P., Belzile, B., Angeles, J.: Trajectory-planning and normalized-variable control for parallel pick-and-place robots. J. Mech. Robot. **11**(3), 031001 (2019)

2. Liu, X.-J., Han, G., Xie, F., Meng, Q., Zhang, S.: A novel parameter optimization method for the driving system of high-speed parallel robots. J. Mech. Robot. **10**(4), 041010 (2018)
3. Briot, S., Caro, S., Germain, C.: Design procedure for a fast and accurate parallel manipulator. J. Mech. Robot. **9**(6), 061012 (2017)
4. Larochelle, P.: Synthesis of planar mechanisms for pick and place tasks with guiding positions. J. Mech. Robot. **7**(3), 031009 (2015)
5. Li, T., Ma, S., Li, B., Wang, M., Li, Z., Wang, Y.: Development of an in-pipe robot with differential screw angles for curved pipes and vertical straight pipes. J. Mech. Robot. **9**(5), 051014 (2017)
6. Dharmawan, A.G., et al.: Design, modeling, and experimentation of a bio-inspired miniature climbing robot with bilayer dry adhesives. J. Mech. Robot. **11**(2), 020902 (2019)
7. Hong, D.W., Ingram, M., Lahr, D.: Whole skin locomotion inspired by amoeboid motility mechanisms. J. Mech. Robot. **1**(1), 1–7 (2008)
8. Asbeck, A.T., Cutkosky, M.R.: Designing compliant spine mechanisms for climbing. J. Mech. Robot. **4**(3), 031007 (2012)
9. Silva, M.F., Machado, J.T., Tar, J.K.: A survey of technologies for climbing robots adhesion to surfaces. In: 2008 IEEE International Conference on Computational Cybernetics, pp. 127–132. IEEE (2008)
10. Cai, J., He, K., Fang, H., Chen, H., Hu, S., Zhou, W.: The design of permanent-magnetic wheeled wall-climbing robot. In: 2017 IEEE International Conference on Information and Automation (ICIA), pp. 604–608. IEEE (2017)
11. Mazumdar, A., Asada, H.H.: An underactuated, magnetic-foot robot for steel bridge inspection. J. Mech. Robot. **2**(3), 031007 (2010)
12. Howlader, M.O.F., Sattar, T.P.: Development of magnetic adhesion based climbing robot for non-destructive testing. In: 2015 7th Computer Science and Electronic Engineering Conference (CEEC), pp. 105–110. IEEE (2015)
13. Faruq Howlader, M.D.O., Sattar, T.P.: Design and optimization of permanent magnet based adhesion module for robots climbing on reinforced concrete surfaces. In: Bi, Y., Kapoor, S., Bhatia, R. (eds.) Intelligent Systems and Applications. SCI, vol. 650, pp. 153–171. Springer, Cham (2016). https://doi.org/10.1007/978-3-319-33386-1_8
14. Zhang, Y., Dodd, T., Atallah, K., Lyne, I.: Design and optimization of magnetic wheel for wall and ceiling climbing robot. In: 2010 IEEE International Conference on Mechatronics and Automation, pp. 1393–1398. IEEE (2010)
15. Ishihara, H.: Basic study on wall climbing root with magnetic passive wheels, pp. 1964–1969 (2017)
16. Seriani, S., Scalera, L., Caruso, M., Gasparetto, A., Gallina, P.: Upside-down robots: modeling and experimental validation of magnetic-adhesion mobile systems. Robotics **8**(2), 41 (2019)

Author Queries

Chapter 88

Query Refs.	Details Required	Author's response
AQ1	This is to inform you that corresponding author has been identified as per the information available in the Copyright form.	
AQ2	As per Springer style, both city and country names must be present in the affiliations. Accordingly, we have inserted the city name "Trieste" in the affiliation. Please check and confirm if the inserted city name is correct. If not, please provide us with the correct city name.	